The Fourth Stokes Parameter for Geolocation in Passive Microwave Remote Sensing from Space

David M. Le Vine, *Life Fellow, IEEE*, Emanuel Dinnat, *Senior Member, IEEE*, Paolo de Matthaeis, *Senior Member IEEE*, and Jinzheng Peng, *Senior Member, IEEE*

***Abstract*—Polarimetric microwave radiometers such as SMAP are capable of measuring the fourth Stokes parameter in brightness temperature over the Earth surface. The value of this parameter is normally small but exhibits sharp spikes when the scene includes large differences in emission from the surface, such occur at land/water boundaries. In this manuscript, it is shown that these spikes can be used to accurately locate coastlines with potential application to geolocation in passive microwave remote sensing from space. Examples are presented using the L-band radiometer on SMAP, first with theory using calculations with the SMAP antenna pattern and orbit and then with SMAP measurements of the fourth Stokes parameter over Madagascar. Using the SMAP data, the coastline is located with a standard deviation less than 2 km. The results are consistent with the conventional approach used for geolocation of the SMAP radiometer footprint.**

***Index Terms*—Passive Microwave Remote Sensing, Geolocation Polarimetric radiometer**

I. Introduction

ACCURATELY confirming the location on the Earth surface of the footprint of a remote sensing instrument in space is an important step in validating the data from that sensor. This can be challenging for passive microwave remote sensing (i.e., microwave radiometers), especially at long wavelengths, because of their relatively poor spatial resolution. One way that has been successful is to use easily identifiable features in the vertically or horizontally polarized brightness temperature such as changes at land-water boundaries and tracking these changes as a function of orientation of the footprint with respect to the boundary. For example, comparing the brightness temperature at coastlines in ascending and descending orbits has been used successfully for AMSR-E [1] and the microwave instruments aboard several NOAA satellites [2]. Determining the inflection point in the change in brightness temperature as the antenna scans across at land-water boundary was used successfully for the radiometers on WindSat [3] and SSMI/S [4] and for the L-band radiometer on SMAP [5]. The advent of fully polarimetric radiometers such as WindSat and SMAP has offered an additional possibility for geolocation: the use the fourth Stokes parameter, Ta4, to identify coastlines. This is a new approach which takes advantage of a strong spike in Ta4 over scenes containing elements with large differences in brightness temperature such as water and land [6]. The objective of this manuscript is to demonstrate, using the L-band radiometer on SMAP, how the fourth Stokes parameter can be used to accurately locate coastlines in the radiometric signature with potential application to footprint geolocation.

A. SMAP

The radiometer on SMAP operates at L-band (1.413 GHz) and is fully polarimetric. It reports the four Stokes parameters TaV, TaH, Ta3, Ta4 called modified Stokes parameters in brightness temperature [7]. The radiometer is conically scanning with a 6-m diameter antenna and circles the Earth in a Sun-synchronous orbit at 685 km altitude [8], [9], [10]. The antenna scans at 14.6 rpm with the antenna boresight at 35.5 degrees with respect to the nadir pointing scan axis. The incident angle at the ground of the antenna boresight is about 40 degrees and the 3 dB contour of the antenna footprint on the ground is 47 km x 36 km [10].

Data is collected in 0.35 ms intervals during which the radiometer observes the scene for 0.30 ms. These sampling intervals are collected into "packets" of 4 measurements each. Four packets (16 measurements looking at the scene) are followed by two packets allocated for internal calibration. This is repeated once and the data (i.e., 8 packets of data looking at the scene) is averaged to form a "footprint" which is the standard data product available to the user. (See Fig. 7 in [10] for a timing diagram.) However, it is possible to access the individual measurements before they are combined into footprints. In the analysis reported here, this data is combined

This paragraph of the first footnote will contain the date on which you submitted your paper for review, which is populated by IEEE. This work was supported in part by the National Aeronautics and Space Administration under Grant 80NSSC18K1443. *(Corresponding author: David M. Le Vine.)*

David M. Le Vine is with the NASA Goddard Space Flight Center, Greenbelt, MD 20771 USA (e-mail: david.m.levine@nasa.gov).

Emmanuel Dinnat is with Cryospheric Sciences Laboratory, NASA Goddard Space Flight Center, Greenbelt, MD 20771 USA, and also with the Center of Excellence in Earth Systems Modeling and Observations, Chapman University, Orange, CA 92866 USA (e-mail: emmanuel.dinnat@nasa.gov)

Paolo de Matthaeis is with the Cryospheric Sciences Laboratory, NASA's Goddard Space Flight Center, Greenbelt, MD 20771 USA, and also with Universities Space Research Association, Columbia, MD 21046 USA (e-mail: paolodemathaeis@nasa.gov)..

Jenzheng Peng J. Peng is with the NASA Goddard Space Flight Center, Greenbelt, MD 20771 USA, and also with the Universities Space Research Association, Columbia, MD 21044 USA (email: jinzheng.peng@nasa.gov).

Mentions of supplemental materials and animal/human rights statements can be included here.

Color versions of one or more of the figures in this article are available online at http://ieeexplore.ieee.org

into ½ footprints (the average of 4 packets = 16 measurements) to improve resolution. The result is an increase in noise, but also an increase by a factor of two in spatial resolution which is important for geolocation. This is a workable compromise between noise and spatial resolution as is shown in the examples to follow. Latitude and longitude are provided for each 0.30 ms measurement and this is averaged to produce the position associated with each ½ footprint of 16 measurements.

B. Fourth Stokes Parameter

The existence of the fourth Stokes parameter, Ta4, requires a phase difference between V and H polarization [11] and natural emission has been reported over surfaces with organized structure such as ocean waves [12], [13] and ice [14] and agricultural fields with row crops [15]. The Ta4 observed by SMAP is small over most surfaces [16] but large spikes occur over scenes with large contrasts in brightness temperature such as at coastlines even though the component pieces (i.e., water or land) have small if any natural Ta4 when viewed by themselves. The spikes are a product of the realities of antenna design (e.g., cross-pol coupling and phase imbalance) and would not be there if the antenna were perfect [6]. The spikes have been observed at L-band by SMAP, by WindSat [17] and in other instruments [18]. The spikes observed by SMAP, and the subject of discussion here, are illustrated in Figs. 1-2.

In Fig. 1 Ta4 is shown for a series of SMAP scans over Madagascar during descending orbit 01470_D. Each ½ footprint is plotted as an individual dot with a color corresponding to the value of Ta4. The spacecraft moves from north to south in Fig 1 and the scans rotate counterclockwise (direction of the arrow). On the top, are examples where the forward portion of the scan crosses Madagascar and on the bottom are the scans where the aft portion of the scan crosses the island. Ta4 is small (green) almost everywhere, over both ocean and land. But at the coastline Ta4 is large and positive (yellow) or negative (blue) depending on whether the scan crosses from land-to-water or water-to-land. The change in sign can be seen comparing the crossing of the East coast with the crossing of the West coast for a given scan. Comparing the two panels in Fig 1 and looking, for example, along the East coastline, shows that the sign does not depend on the coastline but only on whether the crossing is land-to-water or water-to-land.

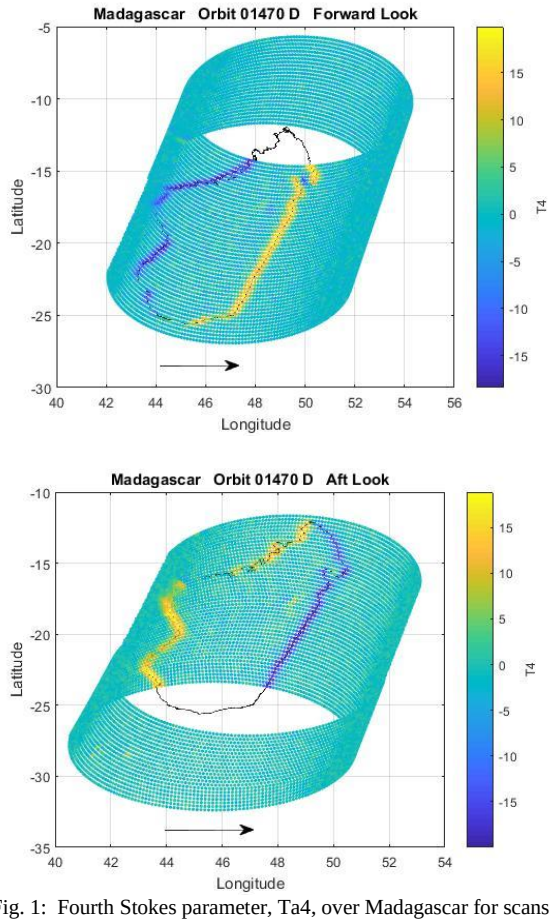

Fig. 1: Fourth Stokes parameter, Ta4, over Madagascar for scans during descending half orbit 01470_D. (Top): Scans with forward portion crossing Madagascar, and (Bottom): Scan with aft portion crossing Madagascar.

Figure 2 shows the spike in more detail. It is a plot of Ta4 as function of scan position for SMAP scan #462 in orbit

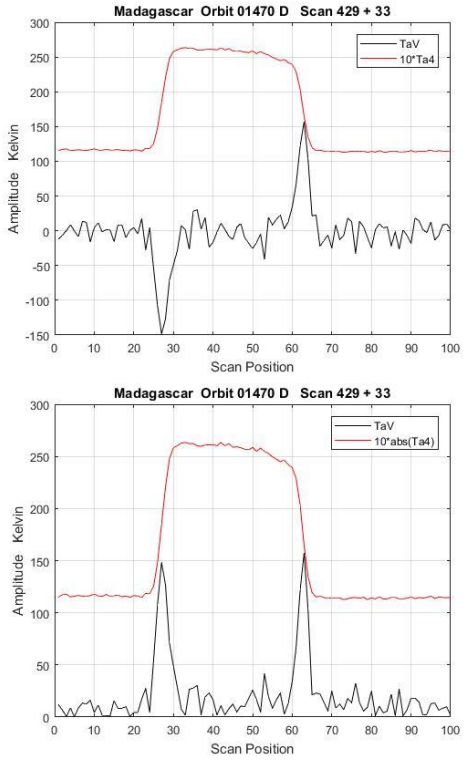

Fig. 2: Example of Ta4 and TaV for scan #462 during descending half-orbit 01470_D. Top and bottom are the same data but the absolute value of Ta4 is shown on the bottom to emphasis the coincidence of peak in Ta4 with transition of TaV at the coastline. Ta4 has been multiplied by 10 to improve visibility.

01470_D. (Ta4 has been multiplied by 10 to make it more visible at this scale.) The scan geometry is shown in Fig 4 (top). Only the portion of the scan crossing southern Madagascar is shown in Fig. 2. The antenna temperature at vertical polarization, TaV, is also plotted (red). The coastline is marked by the large changes in TaV which goes from TaV ≈ 100 over water to TaV ≈ 250 over land. From the panel on the top, it is clear that the sign of the spike depends on whether the antenna moves from land-to-water (positive) or water-to-land (negative), and in both cases the spike lines up well with the coastline. The alignment with the coastline is easier to see in Fig 2 (bottom) where the absolute value of Ta4 is shown to emphasize its correlation with the change in TaV at the coastline.

These characteristics of Ta4 are not unique to SMAP nor to L-band. Spikes in Ta4 at the coastline have been observed in the polarimetric radiometer on WindSat operating at 18 GHz [17].

C. This Manuscript

The objective of this manuscript is to show that the spike in Ta4 at land-water boundaries can be used to accurately locate the boundary, and because of this, Ta4 has potential for use in geolocation of the radiometer footprint. In Section II a SMAP radiometer computer simulator is used to show that in the ideal case (no noise) the spike lines up precisely with the land-water boundary. In Section III, an approach is outlined to use real data to locate the coastline with sub-pixel accuracy. Then in Section IV, this approach is applied to real SMAP data over Madagascar. The accuracy and limitations are discussed in Section V where it is shown that the accuracy depends weakly on the angle of approach to the coastline. In Appendix A an example is presented to show that the locations are consistent with the approach adopted by [5] in the original geolocation of the SMAP radiometer footprint. Also, in Appendix A, the SMAP simulator is used to show that using the inflection point of TaV (or TaH) to identify the boundary as done by [5] has the same dependence on angle of approach at the boundary as Ta4.

II. THEORY

A. Simulator

It is clear from Figs 1-2 that spikes in Ta4 occur at the coastline. To determine how well they actually align with the coastline, an idealized case will be examined first using a computer simulator developed for SMAP. This simulator was initially developed for Aquarius [19] and used as part of calibration [19],[20]. It was later adapted for SMAP where it plays a similar role for calibration (calibration is achieved when the actual signal matches the "expected signal" determined by the simulator [21],[22]). The simulator consists of two parts, a forward radiative transfer model to compute the radiation from the surface arriving at the spacecraft, and a model for the sensor consisting of the sensor antenna pattern, its orientation and movement in space and equations relating the antenna output (antenna temperature) due to the incident radiation [6],[23],[24]. The simulator calculates the L-band radiation at the spacecraft and integrates this radiation over the radiometer antenna pattern keeping track of orientation as the antenna scans and the spacecraft travels in its orbit in space. The simulator output includes all four Stokes parameters. The simulator is currently being used as part of the cold sky calibration of SMAP in which the measured signal while looking at cold sky is compared with the signal predicted by the simulator [21],[25].

As a first step in evaluating the usefulness of Ta4 for geolocation, it will be examined under idealized conditions with no noise and no issues associated with propagation such as attenuation or Faraday rotation. The effects of Faraday rotation are small (see Section VI.A of [Le Vine et al, 2021]). The real case is addressed later using actual SMAP data. For the ideal case, the simulator is used in a stripped-down mode including only radiation from the surface and ignoring issues in radiative transport from surface to sensor that are normally important at L-band such as Faraday rotation, cosmic background radiation, and attenuation through the atmosphere. In addition, the surface has been idealized to consist of ocean and land each with a constant, spatially homogeneous brightness temperature and assuming a perfectly straight coastline. The ocean surface is flat (zero windspeed) with constant temperature and salinity. Likewise, the land is flat with no roughness or vegetation canopy and with fixed temperature and soil moisture. However, the actual SMAP antenna pattern is kept, which is critical for modelling the fourth Stokes parameter, and the scan geometry and orbit parameters of SMAP are also kept in the simulation.

B. Example

Figure 3 is an example from the simulation. The panel on the bottom shows TaV and Ta4 during a complete scan at a land-water boundary (the scene is half water and half land). The scan starts over land and crosses from land to water near scan index 200 and then back to land near scan index 952. (In the simulator there are 1200 computations per scan corresponding to one computation every 0.3 degrees.) The land-water transitions are evident in the large changes in TaV, and each time the scan crosses the land-water boundary there are corresponding spikes in Ta4.

The top panel in Fig. 3 is an expanded view of the water-to-land transition near scan position 952. The solid black curve is Ta4 and the solid red curve TaV. The dashed black curve is the land-water mask (100 for land and 0 for water). The important point in this example is that the peak of the spike in Ta4 lines up precisely with the boundary between land and water (vertical dashed-dot line). The alignment is to within the accuracy of the sampling of the simulation (which is the difference in spacing between the mask value of 100 and the mask value at 0 at the land-water transition). In contrast to the spike in Ta4, the change in TaV is a gradual transition from its value over water

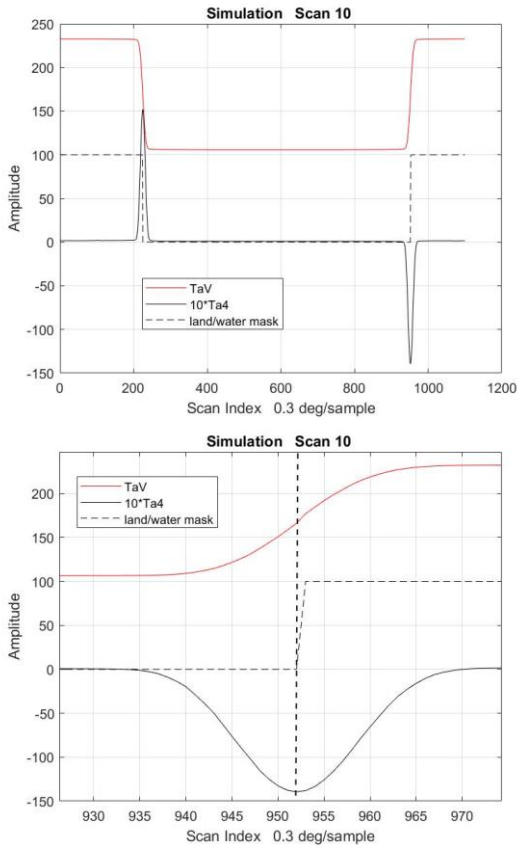

Fig. 3: Example from the simulation of Ta4 (black) and TaV (red) at a land water boundary. Top: Full scan; Bottom: Expanded view showing the crossing at scan position 952 in more detail. The land water mask is the dashed line.

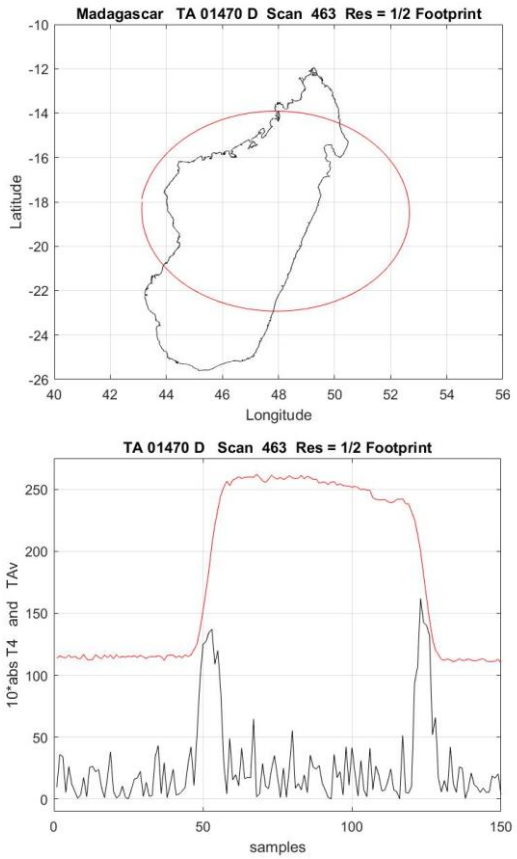

Fig. 4: Example of Ta4 for SMAP scan #463 over Madagascar during half-orbit 01470_D using half-footprint resolution. Top: location of footprint boresight on the ground during this scan (red); Bottom: absolute value of 10*Ta4 (black) and TaV (red) during the southern crossing (forward look).

(about 100 K) to it value over land (about 230 K). This is the result of the convolution of the SMAP antenna pattern with the scene which is a step-function in brightness temperature.

The excellent agreement of the peak of the spike in Ta4 with the actual location of the land-water transition, suggests that it can be used in geolocation of the footprint of sensors like SMAP. The peak is well defined and gives a more obvious location of the boundary than the changes in TaV or TaH. Although this is an idealized case, it is shown below that Ta4 can be used to locate the coastline in the real world using the SMAP radiometer measurements.

III. Approach

An obvious problem in real life is that Ta4 is noisy and because of noise the peak is not immediately obvious. This can be seen in Fig. 2 and is illustrated again Fig. 4 which shows data from the same SMAP scan over Madagascar in higher resolution. The location of the antenna boresight during the scan is shown on the top and on the bottom is shown TaV (red) and the absolute value of Ta4 (black). Ta4 has been multiplied by 10 to make it easier to see and the absolute value taken to help compress the scale (i.e., eliminate the need to also plot large negative values as in Fig. 2). The data presented in Fig. 4 is at half-footprint resolution (i.e., 2 samples per SMAP footprint) whereas the data in Fig. 2 is at full footprint resolution. The scan in Fig. 4 starts at about (Lat -18 deg, Lon 43 deg) over water, and proceeds counterclockwise, crossing Madagascar for the first time in the south near Lat -21 deg. The data in the bottom panel of Fig 4 are from this southern portion of the scan.

It is clear from these examples that the noise in Ta4 at the ½ footprint resolution is significant. Although the spike aligns with the land-water transition, the precise location of the peak is not well defined. Using the full-footprint data (Fig. 2) reduces noise but there is still enough noise to make the location of the peak uncertain, and in that case spatial resolution has been decreased by half.

To identify the peak of the Ta4 spike in the presence of noise, the following steps are taken: First, a smooth curve is fit to the

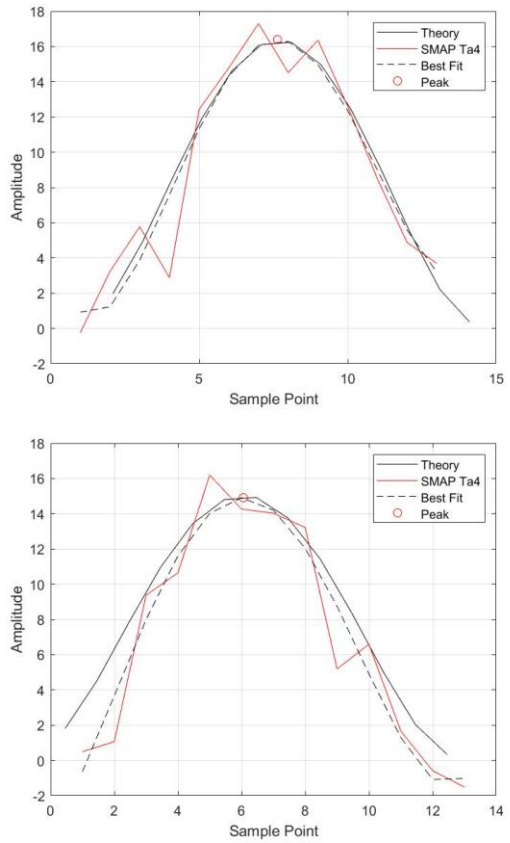

Fig. 5: Two examples of Ta4 (red) from SMAP together with the best fit (dashed) and a scaled version of Ta4 from theory (black). Scan 463 is on the bottom and scan 453 is on the top both from half orbit 01470_D. The "o" indicates the calculated peak.

Ta4 spike; Then, the peak is identified by differentiating this curve and solving for the zero in the derivative.

This is illustrated in Fig. 5 which shows two examples of the fitting. The red curve is the Ta4 reported by SMAP, and the dashed curve is the fit to this data using a 4th order polynomial and the Matlab routine "polyfit". The horizontal axis is the sample number. In each example, 13 samples (SMAP half-footprints) were used to represent Ta4. The fit is only weakly dependent on the number of samples (i.e., adding a sample on each end doesn't change the fit noticeably) although it is necessary that the chosen samples contain the spike in Ta4.

As a check that the fitted curve is reasonable, a curve representing the Ta4 spike from the simulator (solid back) has been included in the figure. The theory is for an ideal case with arbitrarily selected brightness temperature, and the amplitude and width have been scaled to fit the data. The sampling rate of the simulated data is also several times higher than the half-footprint available with SMAP data. Despite these differences the agreement of the best fit and theory is reasonable, and close to the data.

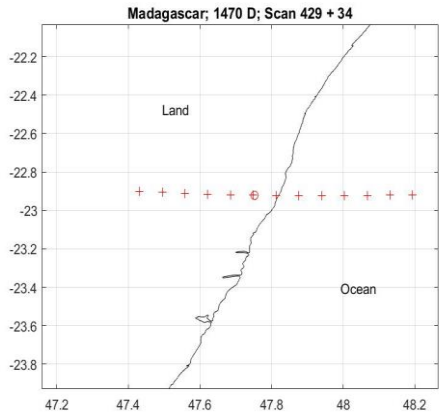

Fig. 6: Example of locating the coastline of Madagascar for scan 463 of orbit 01470_D. The "+" indicated the location of the radiometer samples along the scan ground track and the "o" indicates the detected coastline location. The scan ground track is shown in Fig 4 (top panel) and the measured Ta4 is given in Fig 5 (bottom panel).

The circles ("o") in Fig 5 indicates the location of the peak identified by setting the derivative of the best fit curve to zero. Applying this procedure to the simulator example shown in Fig. 3 results in a location lying at the peak of the spike and on the vertical dashed line.

IV. Application to Madagascar

As an illustration of the potential for using Ta4 to locate coastlines, the procedure outlined above was applied to SMAP observations over Madagascar. The East coast of Madagascar is relatively linear and, it is one of the coastlines used for the geolocation of the SMAP radiometer footprint after its launch [5] and it is currently being used to revisit that geolocation.

Figure 6 shows the results of the geolocation applied to scan 463 of the descending half orbit 01470_D, which is one of the set currently being used to re-evaluate the geolocation of the SMAP radiometer footprint and also used by [5] in the original geolocation of the SMAP radiometer. The location of the antenna boresight during the scan as reported in the SMAP data is shown on a map in Fig. 4 (top). The scan rotates counterclockwise, and the geolocation is done using the crossing of the Eastern coastline near Lat 23 S and Lon 48 E. The Ta4 at this crossing is shown in Fig. 5 (red curve, bottom panel) together with the best fit (dashed line) plotted at the sample points. The red circle indicates the peak as determined from the best fit polynomial (by computing the derivative and solving for the null). Figure 6 is an expanded view of the scan at the eastern coastline showing the location of the half-footprint samples used in the location algorithm ('+") and the point detected as the coastline ('o"). The location of the

samples "+" is obtained by averaging the latitude and longitude of the 16 full-band 0.3 ms observations that comprise the half-footprint. The "o" indicates the location of the peak of Ta4 as determined from the derivative of the best fit. The 13 samples ("+") shown in Fig. 6 correspond to the 13 values of Ta4 shown in Fig 5 (bottom) and used to determine the fit. The sample identified as #1 in Fig. 5 on the horizontal axis corresponds to the "+" on the far left in Fig 6 (i.e., the scan is moving from left to right).

This process was applied to several scans in three different orbital passes over Madagascar with consistent results. This is illustrated in Fig 7 which shows the results from 9 scans across the Madagascar coast during the descending half-orbit 01470_D. An expanded view of the same scans is shown on the bottom. As in Fig 6, the location of the coastline determined using Ta4 is identified with the circle "o" and the "+" are the location of the data samples that were used in the geolocation. The locations, "o", are consistently west of the actual coastline. As a check, this exercise was run for two other descending half-orbits, 01740_D and 01587_D with similar results. The mean distance between the coastline and the locations was similar for all three cases. The results are shown in Fig 8 which is a plot of the distance between the located coastline (the "o") and the actual coastline (map) for the nine scans in each half-orbit. The mean difference for all examples was 3.65 km (the spacing between half-footprints is 6 km).

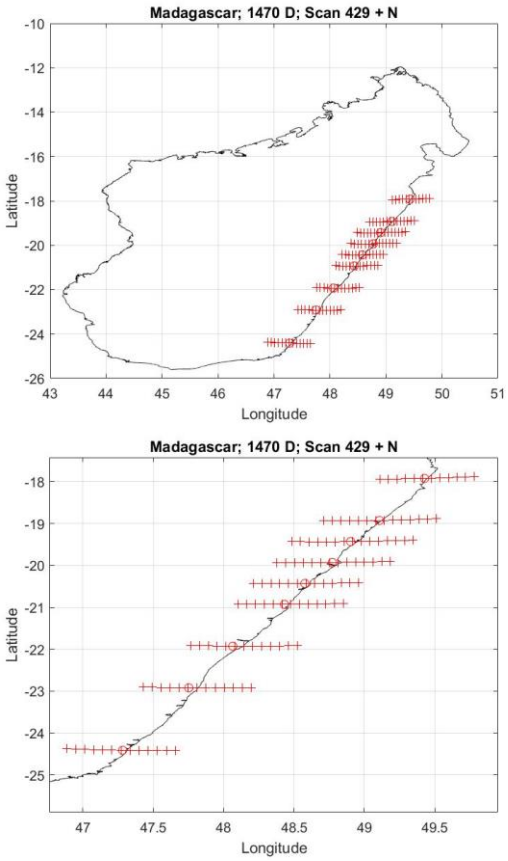

Fig. 7. Geolocations with forward looking portion of scans during orbit 01470_D over Madagascar. The coastline geolocations are indicated with the circle ("o") and the location of the SMAP half-footprint data used in the geolocation is given by the crosses ("+"). Summary on the top and expanded view on the bottom.

V. Discussion

A. Accuracy

As a check on the results from Madagascar, the geolocations in Section IV above were also done for the aft portion of those scans in the three descending passes, 01470_D, 01587_D and 01740_D which cross the east coast of Madagascar. The scans in pass 01470_D with forward-looking portions that cross the coast are those shown in Fig. 1 (top) and the scans in this pass with aft portions crossing the coast are the ones used to produce Fig. 1 (bottom). The geometry is almost identical for the other two descending passes, 01587_D and 01740_D. The locations found with all these scans are consistent: The locations are similar relative to the coastline for all the scans in a given pass and the locations are about the same for each of the three passes. But the coastline detections are much closer to the coastline for the aft portion of the scans than for the forward portion of the scans. The mean distance between the detected coastline and the actual coastline using the forward portion of the scans is 3.64 km to the west of the coastline (Fig. 8); but using the aft portion of the scans, the locations are close to and on both sides of the coastline with a mean difference of 0.25 km west (the standard deviation is 1.81 km).

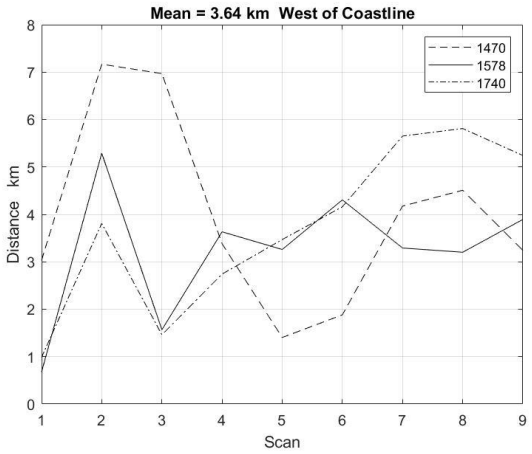

Fig 8: Distance between coastline located using SMAP data and the actual coastline for orbits 01470, 01587 and 01740. The mean distance for all cases is 3.64 km.

In an ideal case, there should be no difference between locations made with the forward portion of the scan or the aft portion of the scan. The sign of Ta4 changes but the shape is

independent of the direction. This has been verified using the simulator (see examples in Fig. 3 and 9). As a check, to see if this difference between forward and aft scans could be associated with the retrieval algorithm, the locations of the coastline were compared with results of an independent study underway to revisit the geolocation of the SMAP radiometer footprint. This study uses the change in antenna temperature and the approach used by [5] in the original SMAP radiometer geolocation to identify the coastline. Good agreement was found between the two approaches with a similar difference between the locations obtained with the forward and aft portion of the scan. (See Appendix A for a comparison.)

The consistency of the results among all scans and the confirmation with the conventional approach using TaV suggests the difference between for and aft portions of the scan is a real feature of the SMAP data and possibly associated with a residual bias in the geolocation of the SMAP radiometer footprint. It is beyond the scope of this manuscript to try to establish the SMAP geolocation with this limited data, but a difference between forward and aft looks could be caused by a small error in the orientation of the axis of the scan or some combination of error in pitch and roll. Initial results using GNSS-R measurements being conducted with the SMAP radar receiver suggest a small error in the pointing of the SMAP antenna boresight (N. Rodriguez-Alvarez and J. Munoz-Martin, private communication).

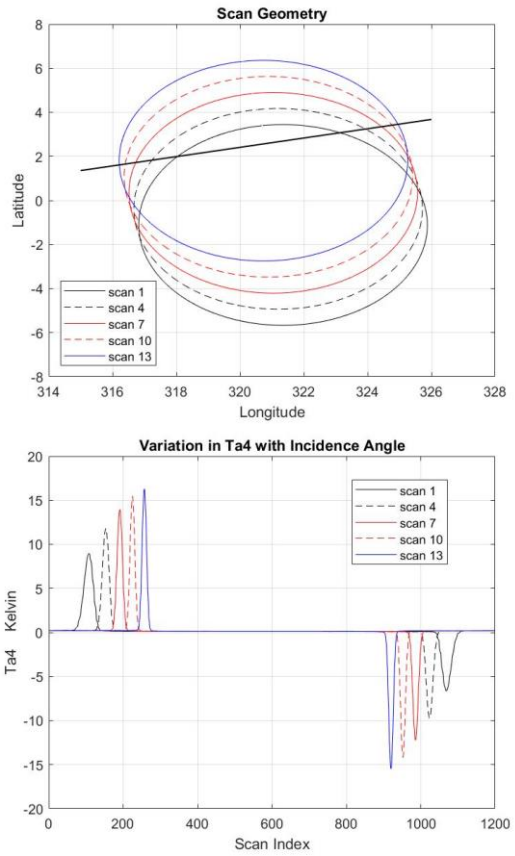

Fig 9. The effect of the crossing angle of the scan at a land/water boundary on Ta4. (Top) Ground track of five scans with respect to the land/water boundary (heavy dark line); water is south and land north of the line. (Bottom) Ta4 for these 5 scans. The crossing angle increases with scan number and is perpendicular for scan #13

Given the possibility of a small residual error in the geolocation of the SMAP radiometer footprint, comparing the locations obtained with the examples above does not provide a reliable estimate of the accuracy of using Ta4 to locate the coastline. However, even if there is no error in the SMAP radiometer geolocation, the mean difference between the coastline and location given using Ta4 and the SMAP data are still very good: a mean error of 3.64 km for the forward scans and mean of 0.25 km for the aft scans with standard deviation of 1.66 km and 1.81 km, respectively. These distances are much less than the 3 dB footprint of the SMAP radiometer and

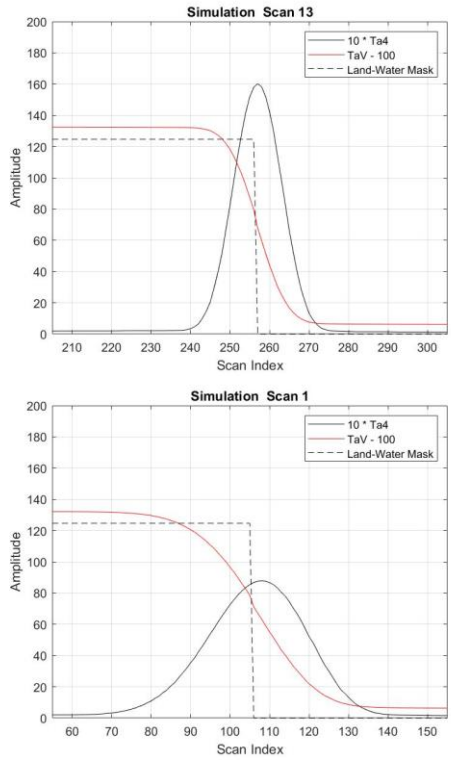

Fig. 10: Expanded view of 10*Ta4 (black), TaV - 100 (red) and the land-water mask (dashed) at a land-water crossing (simulation). (Top) Scan #13 crossing perpendicular to boundary; (Bottom) Scan #1 crossing boundary at about 60 degrees.

better than the spacing between the half-footprints (about 6 km) used in the analysis. The error reported in the SMAP geolocation by [5] was ±2 km which is larger than the standard deviation using Ta4 in these examples.

B. Issues

One obvious limitation of the approach outlined here is the

shape of the coastline. If it is irregular and/or includes large bays or inlets, the shape of the spike in Ta4 will be impacted and errors can occur. But of course, this is also a limitation of conventional approaches using TaV or TaH and this is the reason the east coast of Madagascar was chosen for original geolocation by SMAP [5]. No irregular or missing spikes were found in the section of coastline employed in this analysis.

Another obvious issue associated with accuracy is the radiometer sample rate. The SMAP data is highly over sampled (32 radiometer measurements which are averaged to produce one "footprint") which provides some room to improve spatial resolution but at the cost of increased noise. In the examples presented here 16 radiometer measurements were used to improve spatial resolution. This increased the noise in the Ta4 spikes as can be seen by comparing Ta4 in Fig. 2 and Fig. 4. The objective here was just to demonstrate the technique, but there is clearly some additional work to be done to determine the optimum trade between noise and spatial resolution with the oversampled data. A similar trade would probably benefit other approaches and it points to the advantage of having oversampled data to work with.

A less obvious limitation is that the accuracy potentially depends on the way the scan intersects the land-water boundary. The ideal case is when the scan intersects the coastline at right angles (i.e., when the red line representing the scan in Fig. 4 (top), or line through the "+" in Fig. 6, is perpendicular to the coastline). When the angle between the scan and coastline decreases, the spike in Ta4 broadens and the amplitude decreases. This is illustrated with the simulator in Fig. 9 which shows several noise-free scans made as the spacecraft moves across a land-water boundary. The path of the antenna boresight on the surface is shown on the top with the land-water boundary indicated by the heavy black line (land is north of the line). The Ta4 for each scan is shown as function of scan angle in the bottom panel. Scan 1 (solid black) is the southern-most scan, and its ground track intersects the land-water boundary at the smallest angle. Scan 13 (solid blue) is the northern-most scan. In this scan the spacecraft nadir location is almost on the land-water boundary and the scan ground track is almost perpendicular to the land-water boundary. The spikes in Ta4 associated with scan 1 (smallest angle of intersection) are the smallest in amplitude and broadest in scan index, and the spikes associated with scan 13 (almost perpendicular) are the tallest and narrowest. In moving from scan 1 to scan 13, the pair of spikes in Ta4 also move closer together because the portion of the scan south of the land-water boundary decreases.

Figure 10 is an expanded view of the transition from land-to-water in scan 13 (top) and scan 1 (bottom). The width of both the Ta4 peak (black) and the TaV transition (red) increase as the angle of intersection of the scan with the land-water boundary decreases. The width of the transition of TaV from water to land is about 30 samples, as indicated by the scan index on the horizontal axis, in Scan 13 (perpendicular incidence) and about 50 samples in Scan 1 (intersection angle of about 60 degrees).

This scaling of the width of Ta4 and TaV with the angle of intersection of the scan with the coastline is a consequence of geometry. For example, imagine the 3 dB contour (or any other level) of the antenna footprint to be a circle. Then, as the footprint crosses perpendicular to the boundary, the transit "time" is determined by the diameter, D, of the contour. However, the time from first contact to last contact at any other angle, φ, is determined by $D/\sin(\varphi)$. The change in amplitude of Ta4 with the angle of intersection is also an issue of geometry, although more complex in this case because the components of the antenna pattern involved in the integration to produce Ta4 comprise two peaks of opposite sign separated by a null (e.g., see Eqns. 2 and Figs 4-5 in [6]).

Two effects contribute to making a perpendicular crossing best. The first is the that decreased amplitude at smaller crossing angles will increase the impact of noise (decrease signal to noise ratio since the noise is not changed). The second is that there is a slight bias in the location of the peak when the crossing is not perpendicular to the boundary. This bias can be seen in Fig 10 (bottom) by comparing the peak of Ta4 (black) with the land/water mask (dashed). The bias is about 3 scan positions or about 2.5 km at the SMAP altitude and scan angle. The bias is the same when the crossing is from water-to-land. There is no noticeable bias when the scan crosses perpendicular to the coast (top panel). This bias also occurs in the inflection point of TaV which also shifts slightly in the same direction as the peak in Ta4 when the angle of intersection with the boundary decreases (see Appendix A). Although the bias is small, the bias together with the decrease in amplitude are probably reasons to look for cases when the angle of intersection with the coastline is close to perpendicular when doing geolocation.

VI. Conclusion

The objective of this manuscript has been to demonstrate that the fourth Stokes parameter, Ta4, can be used to locate land-water boundaries such as coastlines and provide an additional way to help validate the pointing and geolocation of the antenna footprint of passive microwave sensors in space.

The fourth Stokes parameter is well suited for geolocation using coastlines because it is very small for uniform scenes and only responds when the scene includes elements with much different brightness temperature such as occurs at coastlines. This behavior occurs because the dominant term in the antenna pattern contributing to Ta4 consists of opposite signed peaks (see Section IV.B in [6]). When the scene is uniform (constant TB), the contribution from the two peaks cancel each other in the integration over the antenna pattern, but when one part of the footprint is over a scene with low brightness temperature

(e.g., ocean) and the other over a scene with high TB (e.g., land), it is possible to have a large difference.

The examples presented here using SMAP radiometer scans over Madagascar demonstrate that the technique works. The standard deviation of the difference between the locations and the actual coastline was 1.66 km using the forward portion of the scans and 1.81 km with the aft portion of the scans. This is better than the spacing between samples used in the algorithm (6 km) and comparable to the accuracy (±2 km) claimed in the geolocation done for SMAP by [5]. The locations, including the difference observed between forward look and aft look are consistent with an independent geolocation currently in progress and using a conventional technique (locating the inflection point in the change in antenna temperature at vertical or horizontal polarization).

Finally, the examples given here are for a radiometer operating at L-band (1.4 GHz), but spikes in Ta4 at coastlines have been reported at 18 GHz from WindSat [17], and [18] reports spikes in Ta4 for a polarimetric radiometer operating at 91 GHz. Both these reports at higher frequency are from instruments using the difference between right-hand and left-hand circular polarization to measure Ta4 as opposed to the direct method used by SMAP [see Appendix A of [6] for a discussion]. The SMAP approach will see spikes when there is a change in Q = TBv – TBh within the antenna footprint [6] and the approach using circular polarization will see spikes when there is a change in I = TBv + TBh within the footprint [18]. The difference in Q and I between land and ocean is reported in Table I at 40 degrees local incidence angle for the frequencies commonly used for remote sensing from space. The differences are relatively stable over this frequency range. Of course, even though spikes may be observed at these frequencies, how well the spikes serve for geolocation will depend on the details of the specific sensor and the approach will have to be tuned to each sensor. But Table I suggests that the potential exists independent of frequency and method of detecting Ta4.

Table I: Example Brightness Temperatures

Frequency		Ocean TB Kelvin		Land TB Kelvin		Difference Land-Ocean	
		Q	I	Q	I	ΔQ	ΔI
1.4 GHz		44	198	57	357	13	161
6 GHz		45	221	57	353	12	142
10 GHz		46	224	57	371	11	147
18 GHz		47	231	57	391	10	160
32 GHz		48	247	55	423	6	176

Ocean: Zhou et al model [27] for dielectric constant with SST = 20 C; SSS = 35 psu; WS = 0 m/s

Land: Dobson model for the dielectric constant as given by [26] with SM = 0.3; Sand fraction = 0..4; Clay fraction = 0.3; bulk density = 1.7 g/cc; T = 23 C; no vegetation; no Roughness

VII. Appendix A

A more conventional approach for locating a land-water boundary is to use the inflection point in the change in the antenna temperature TaV or TaH as the radiometer crosses the boundary as the marker for the coastline. This works well in the idealized case as is shown in the Fig. A.1. The results in Fig. A.1 were obtained with the simulator (Section II.A above) using uniform ocean and land (i.e., each with constant TB) and no noise. The solid line is the antenna temperature at vertical polarization, TaV, and the dashed line is the land/water mask (water is zero). To compute the inflection point, a fifth order polynomial is fitted to TaV and then differentiated twice. The second derivative is shown in red. The inflection point is where this curve crosses zero. The panel on the top is for a case when the scan crosses perpendicular to the coastline and the panel on the right is for an intersection of about 60 degrees. When the intersection is perpendicular (top), the inflection point aligns precisely with the boundary (i.e., where the mask changes from water to land). When the intersection is oblique (bottom panel of Fig A1), the transition takes longer as TaV is stretched out over more scan positions. The end points, ocean and land, are fixed so that magnitude of the change in TaV does not change. However, because the change in TaV is slower at oblique intersection, the second derivative (red) has a smaller peak amplitude. In both cases, the inflection point is a good

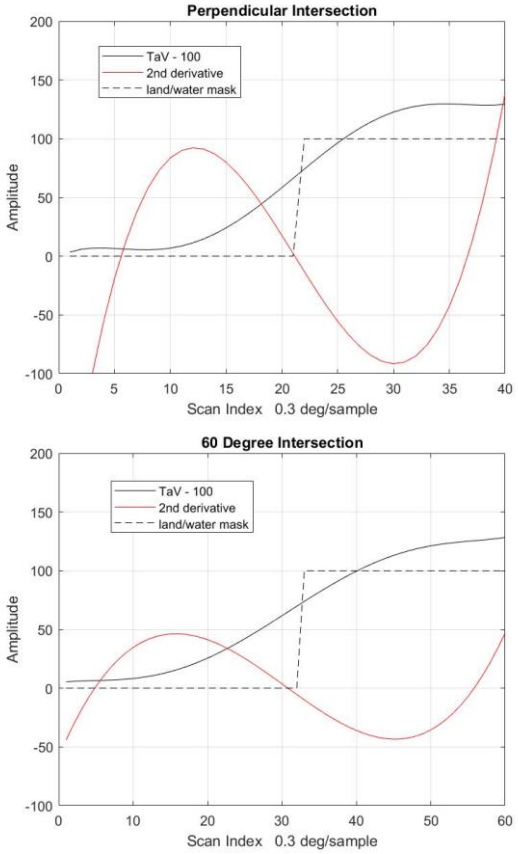

Fig. A1: Geolocation using the inflection point: TaV (solid black), second derivative (red) and land/water mask (dashed). TaV is from the simulator. Top: Scan perpendicular to the boundary; Bottom: Scan intersection angle approximately 60 degrees.

indication of the boundary. But in the case when the scan is not perpendicular to the boundary, there is a small bias toward the water side. This is the same effect as noticed in the case of Ta4 (Section V.B above). Both TaV and Ta4 broaden as the scan intersects the boundary at smaller angles and the metric for locating the boundary in each case, amplitude of Ta4 and second derivative of TaV, decrease. This makes them both more likely to be impacted by noise compared to incidence perpendicular to the boundary.

A variation of the approach using the inflection point was used in the post-launch verification of the geolocation of the SMAP radiometer footprint [5]. The difference is that rather than fitting a polynomial to TaV and differentiating as above, a curve with a fixed shape was fitted to the data. This procedure is being repeated as this manuscript is being prepared by one of the co-authors (J. Peng). A comparison of results obtained using this procedure with the approach using Ta4 described in this manuscript is shown in Fig. A2 for the aft scans of orbit 01470_D over Madagascar. The red asterisks ("*") are the geolocation using Ta4 and the green circles ("o") are the geolocation using the inflection point of TaV obtained with the approach used in [5] but redone by J. Peng as part of the new analysis. The comparison for the forward portion of the scans is on the top and a comparison for aft portion of scans is on the bottom. The locations from the two approaches are in reasonable agreement, and the difference between locations using the forward and aft portion of scans is present in both approaches. In particular, the red asterisks and green circles are consistently west of the coastline (Fig. A2, top) using the forward portion of the scans and are very close to the coastline using the aft portion of the scans (Fig. A2, bottom).

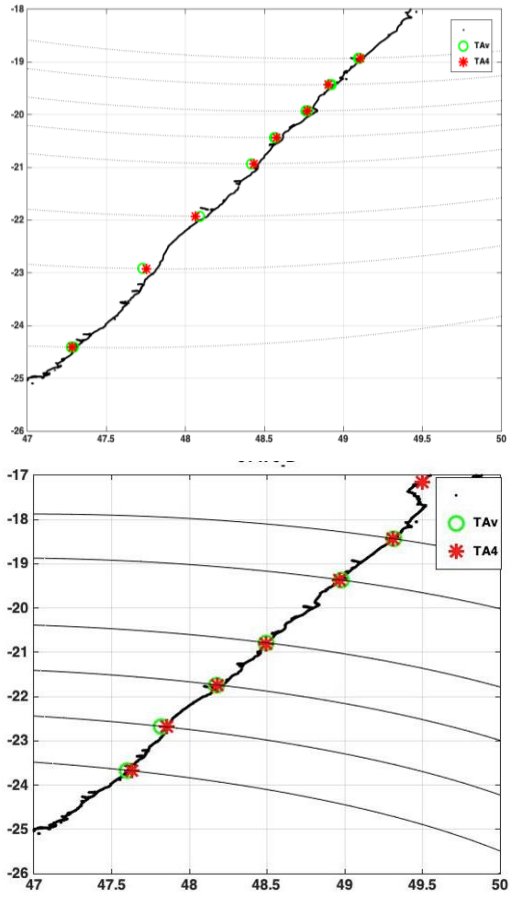

Fig. A2: Comparison of geolocation using Ta4 (red) with traditional method using the inflection point of TaV (green) for forward portion of scans (top) and aft portion of scans (bottom) for orbit 01470_D over the east coast of Madagascar. The solid lines represent the ground track of the SMAP scan. Land (Madagascar) is on the left (west) and ocean on the right (east) of the coastline.

VIII. References

[1] H. Wiebe, G. Heygster and L. Meyer-Lerbs, "Geolocation of AMSR-E data," IEEE TGRS, 46, 3098–3103, October 2008.

[2] I. Moradi, H. Meng, R.R. Ferraro and S. Bilanow, "Correcting Geolocation Errors for Microwave Instruments aboard NOAA Satellites", IEEE TGRS, 51, 3625, June, 2013; doi 10.1109/TGRS.2012.2225840

[3] W.E. Purdy, et al., "Geolocation and pointing accuracy analysis for the WindSat sensor," IEEE TGRS, 44, 496-505, March 2006; doi 10.1109/TGRS.2005.858415

[4] G.A Poe, E.A. Uliana, B.A. Gardiner, T.E. vonRentzell and D.B. Kunkee, "Geolocation error analysis of the special sensor microwave imager/sounder," IEEE Trans. Geosci. Remote Sens., vol 46, 913-922, April 2008; doi 10.1109/TGRS.2008.917981

[5] G. De Amici, J. Piepmeier, J. Peng, "Geolocation Results for the SMAP Passive Instrument, MicroRad 2016.

[6] D.M. Le Vine, Y. Soldo and E.P. Dinnat, Spurious Signal in SMAP Fourth Stokes Parameter, IEEE Transactions on Geoscience and Remote Sensing, Vol. 59 (#11), pp 9472-9485, Nov., 2021 DOI 10.1109/TGRS.2020.3035335.

[7] J. Randa et al., "Recommended terminology for microwave radiometry," Nat. Inst. Standards Technol., United States Dept. Commerce, Washington, DC, USA, Tech. Note. 1551, Aug. 2008.

[8] D. Entekhabi, S. Yueh, P. E. O'Neill, and K. H. Kellogg, SMAP Handbook. Pasadena, CA, USA: JPL, Jul. 2014.

[9] D. Entekhabi, E. G. Njoku, P. O'Neill, K. Kellogg, W. Crow, W. Edelstein, et al. (2010). The soil moisture active and passive (SMAP) mission, Proceedings of the IEEE, 98(5), 704–716.

[10] J. R. Piepmeier et al., "SMAP L-band microwave radiometer: Instrument design and first year on orbit," IEEE Trans. Geosci. Remote Sens., vol. 55, no. 4, pp. 1954–1956, Jan. 2017, doi: 10.1109/TGRS.2016.2631978.

[11] S. H. Yueh, "Modeling of wind direction signals in polarimetric sea surface brightness temperatures," IEEE Transactions on Geoscience and Remote Sensing, 35(6), pp.1400-1418, 1997.

[12] S. H. Yueh, William J. Wilson, Fuk K. Li, Son V. Nghiem and William B. Ricketts, Polarimetric Brightness Temperatures of Sea Surfaces Measured with Aircraft K- and Ka-Band Radiometers, IEEE Transactions on Geoscience and Remote Sensing, 35(5), pp.1177-1187, 1997..

[13] P. W. Gaiser, K. M. St. Germain, E. M. Twarog, G. A. Poe, W. Purdy, D. Richardson, W. Grossman, W. L. Jones, D. Spencer, G Golba, J. Cleveland, L. Choy, R. M. Bevilacqua, and P. S. Chang, The WindSat Spaceborne Polarimetric Microwave Radiometer: Sensor Description and Early Orbit Performance, IEEE Transactions on Geoscience and Remote Sensing, 42(11), pp.2347-2361, doi 10.1109/TGRS.2004.836867

[14] L. Li, P. Gaiser, M. R. Albert, D. G. Long and E. M. Twarog, WindSat Passive Microwave Polarimetric Signatures of the Greenland Ice Sheet, IEEE Transactions on Geoscience and Remote Sensing, 46(9), pp.2622-2631, 2008, doi 10.1109/TGRS.2008.917727

[15] P. S. Narvekar, T. J. Jackson, R. Bindlish, Li Li, G. Heygster, and P. Gaiser, Observations of Land Surface Passive Polarimetry With the WindSat Instrument, IEEE Transactions on Geoscience and Remote Sensing, 45(7), pp.2019-2028, doi 10.1109/TGRS.2006.886963

[16] Y. Soldo, D. M. Le Vine and E. Dinnat, SMAP Observations of the Fourth Stokes Paramater at L-Band, International Geoscience and Remote Sensing Symposium (IGARSS), Yokahama, Japan, 2019

[17] S. W. Ellingson and J. T. Johnson, "A polarimetric survey of radiofrequency interference in C-and X-bands in the continental United States using WindSat radiometry," IEEE Trans. Geosci. Remote Sens., vol. 44, no. 3, pp. 540–548, Mar. 2006.

[18] A. Duric, B. Hitz, A. Murk and C. Matzler, Correction of the Off-Axis Reflector Beam Squint in Passive Images of the Fourth Stokes Parameter, The Second European Conference on Antennas and Propagation, EuCAP 2007

[19] D.M. Le Vine, E.P. Dinnat, S. Abraham, P. de Matthaeis, F.J. Wentz, "The Aquarius Simulator and Cold-Sky Calibration", IEEE Transactions on Geoscience and Remote Sensing, Vol. 49 (#9), pp 3198-23210, September, 2011 DOI 10.1109/TGRS.2011.2161481.

[20] E. P. Dinnat, D. M. Le Vine, J. R. Piepmeier, S. T. Brown, and L. Hong, "Aquarius L-band radiometers calibration using cold sky observations," IEEE J. Sel. Topic Appl. Earth Observ. Remote Sens., vol. 8, no. 12, pp. 5433–5449, 2015. DOI 10.1109/JSTARS.2015.2496362.

[21] J. Peng, S. Misra, J. R. Piepmeier, E. P. Dinnat, D. Hudson, D. M. Le Vine, et al., "Soil moisture active/passive (SMAP) L-band microwave radiometer post-launch calibration," IEEE Trans. Geosci. Remote Sens., vol. 55, no. 9, pp. 5339–5354, Sep. 2017; doi 10.1109/TGRS.2017.2705342

[22] J. Peng , S. Misra, J. R. Piepmeier, E. P. Dinnat, S. H. Yueh, T. Meissner, D. M. Le Vine, K. E. Shelton, A. P. Freedman, R. S. Dunbar, S.K. Chan, R. Bindlish, G. De Amici, P.N. Mohammed, L. Hong, D.Hudson, and T. Jackson, Soil Moisture Active/Passive (SMAP) L-Band Microwave Radiometer Post-Launch Calibration Upgrade, IEEE J. of Selected Topics in Applied Earth Observations and Remote Sensing, Vol. 12, #6, June 2019, pg 1647 doi: 10.1109/JSTARS.2019.2902492.

[23] D. M. Le Vine, S. D. Jacob, E. P. Dinnat, P. de Matthaeis, and S. Abraham, "The influence of antenna pattern on Faraday rotation in remote sensing at L-band," IEEE Trans. Geosci. Remote Sens., vol. 45, no. 9, pp. 2737–2746, Sep. 2007; doi 10.1109/TGRS.2007.898237

[24] E.P. Dinnat and D.M. le Vine, "Effects of the Antenna Aperture on Remote Sensing of Sea Surface Salinity at L-Band". IEEE Transactions on Geoscience and Remote Sensing, 45(7), 2051–2060, 2007 doi.org/10.1109/TGRS.2007.890807.

[25] E.P. Dinnat and D.M. Le Vine, SMAP Calibration Using Cold Sky Calibration, International Geoscience and Remote Sensing Symposium, IGARSS 2022, Kuala Lumpur, Malaysia, July 17-22, 2022.

[26] F.T. Ulaby and D.G. Long, Microwave Radar and Radiometric Remote Sensing, Univ Michigan Press, Ann Arbor, 2014 (Chapter 4.8).

[27] Y. Zhou, R.H. Lang, E.P. Dinnat and D.M. Le Vine, Seawater Debye Model Function at L-Band and Its Impact on Salinity Retrieval from Aquarius, IEEE Trans. Geosci. And Remote Sensing, Vol 59, No 10 October, 2021, doi: 10.1109/TGRS.2020.3045771.